Review



# Telmisartan-Induced Alteration of Voltage-Gated $Na^+$ Currents: Integrated Experimental and In Silico Approaches

Sheng-Nan Wu *, Rasa Liutkevičienė, Vita Rovite, Chung-Hung Tsai, Sheng-Che Lin

Posted Date: 6 March 2026

doi: 10.20944/preprints202603.0533.v1

Keywords: telmisartan; voltage-gated $Na^+$ channel; current kinetics; membrane potential; modeled cell; excitable cell

 doi:10.20944/preprints202603.0533.v1



*Review*

# Telmisartan-Induced Alteration of Voltage-Gated $Na^+$ Currents: Integrated Experimental and In Silico Approaches

**Sheng-Nan Wu [1,*], Rasa Liutkevičienė [2], Vita Rovite [3], Chung-Hung Tsai [4,5] and Sheng-Che Lin [6]**

[1] Department of Research and Education, An Nan Hospital, China Medical University, Tainan, Taiwan
[2] Laboratory of Ophthalmology, Institute of Neuroscience, Lithuanian University of Health Sciences, Eivenių Str. 2, LT-50161 Kaunas, Lithuania
[3] Latvian Biomedical Research and Study Centre, Ratsupites Str. 1-k1, LV-1067 Riga, Latvia
[4] Institute of Allied Health Science, College of Medicine, National Cheng Kung University, Tainan, Taiwan
[5] Department of Family Medicine, An Nan Hospital, China Medical University, Tainan, Taiwan
[6] Department of Plastic Surgery, An Nan Hospital, China Medical University, Tainan, Taiwan
* Correspondence: 071320@tool.caaumed.org.tw

**Abstract**

Telmisartan (TEL) is a non-peptide, orally administered antihypertensive agent primarily known as angiotensin II type 1 (AT1) blocker. In this review, we provide a detailed overview of how TEL modulates voltage-gated $Na^+$ current ($I_{Na}$) and affects action potential (AP) firing behavior. TEL exerts differential stimulatory effects on the peak and late components of $I_{Na}$ when subjected to brief depolarizing pulses across a range of cell types, such as mHippoE-14 hippocampal neuron, cultured dorsal root ganglion neurons, and HL-1 atrial cardiomyocytes. TEL can augment the inactivating (persistent) $I_{Na}$ elicited by ascending long ramp pulse in mHippoE-14 cells. By using a parvalbumin-expressing interneuron-based modeled cell combined with bifurcation analysis, it is possible to predict how applied current influences subthreshold oscillations and the generation of somatic spiking in the presence of TEL. According to the Hodgkin-Huxley model, mimicking the action of TEL—characterized by an increased peak amplitude of $I_{Na}$ and a slowed inactivation time course—leads to the emergence of periodic oscillations in membrane potential. Using a Markovian process, a separate model can also be mathematically constructed, showing that changes in certain rate constants can simulate the effect of TEL on $I_{Na}$ in cardiac cells. The molecular docking prediction between TEL and the Nav1.7 channel was made by expected formation of hydrophobic interactions as well as hydrogen bonding. Beyond its antagonistic action on AT1 receptor and agonistic activation of peroxisome proliferator-activator-γ, the direct stimulation of $I_{Na}$ may also contribute to its modulation of AP firing in various excitable cells. Current evidence supports TEL's modulatory impact on Nav channel activity and cellular excitability, while also acknowledging that the mechanism—whether direct or indirect—remains under investigation.

**Keywords:** telmisartan; voltage-gated $Na^+$ channel; current kinetics; membrane potential; modeled cell; excitable cell

## 1. Introduction

Telmisartan (TEL, Micardis®, $C_{33}H_{30}N_4O_2$, 2-(4-{[4-methyl-6-(1-methyl-1H-1,3-benzodiazol-2-yl)-2-propyl-1H-1,3-benzodiazol-1-yl]methyl}phenyl)benzoic acid; IUPAC name: 4′-[(1,4′-Dimethyl-2-propyl[2,6′-bi-1H-benzimidazol]-1′-yl)methyl]-[1,1′-biphenyl]-2-carboxylic acid) is recognized as a non-peptide, orally active blocker of the angiotensin II type 1 (AT1) receptor [1–4]. TEL, marketed under the brand name Micardis® by Boehringer Ingelheim, was approved by the U.S. Food and Drug

 doi:10.20944/preprints202603.0533.v1



Administration in 1998, and it received marketing authorization in the European Union in 1998. The trade name of TEL may vary depending on the country and manufacturer.

TEL belongs to a newer class of drugs indicated for the treatment of hypertension and various cardiovascular disorders. Its modified aromatic moiety, as shown in **Figure 1**, contributes to enhanced lipophilicity, enabling efficient penetration into the central nervous system [5]. Owing to its agonistic interaction with peroxisome proliferator-activated receptor-γ (PPAR-γ) [6–9], TEL exhibits notable metabolic and anti-inflammatory properties that transcend its primary function in regulating blood pressure [5,10]. Additionally, oral administration of TEL has been shown to markedly enhance cognitive performance and mitigate memory impairments in both preclinical animal studies and human subjects [5,7,8,11–23].

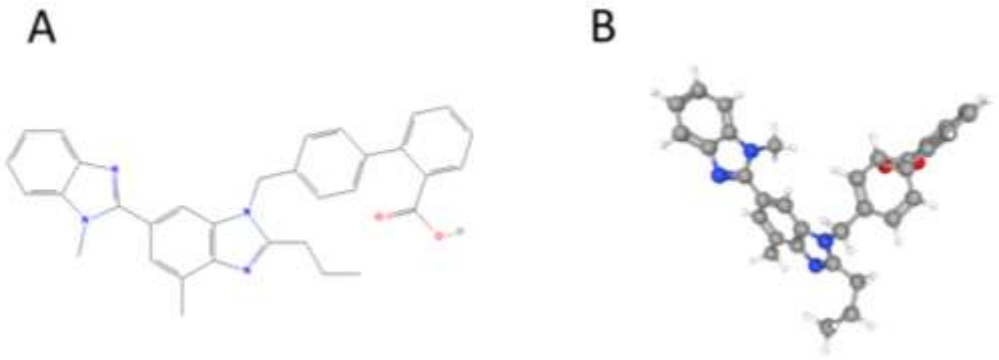


**Figure 1.** Chemical structure of telmisartan (TEL; compound CID: 65999). **(A)** Two-dimensional representation highlighting the molecular framework, including multiple aromatic benzene rings and functional groups. **(B)** Three-dimensional structure of the TEL molecule. Carbon atoms are depicted in gray, hydrogen in white, nitrogen in blue, and oxygen in red. Notably, the molecule's complex and bioactive configuration, characteristic of pharmaceutical compounds, is defined by its multiple aromatic rings, aliphatic chains, and a carboxyl group (COOH).

Voltage-gated $Na^+$ (Nav) channels play a crucial role in initiating and propagating actions potentials in electrically excitable cells [24]. In mammals, there are nine distinct Nav channel α-subunit isoforms, designated Nav1.1 through 1.9, which correspond to the genes *SCN1A* through *SCN5A* and *SCN8A* though *SCN11A*. These channel isoforms are widely distributed throughout excitable tissues, such as the central and peripheral nervous systems, skeletal muscles, endocrine glands, and cardiac tissue [24–26].

During depolarization, Nav channels rapidly transition from a closed (resting) state to an open state, followed by inactivation. The non-inactivating, or persistent, $Na^+$ current ($I_{Na(NI)}$) represents a component of the whole-cell $Na^+$ current ($I_{Na}$) that remains functionally active throughout the repolarization phase of the action potential (AP). Unlike transient Nav channels, which inactivate quickly, these non-inactivated Nav channels continue to conduct a small but significant inward $I_{Na}$ over a longer period [27–31]. $I_{Na(NI)}$ play an important role in modulating membrane excitability and shaping the firing patterns of APs in various cell types, including neurons and endocrine cells.

By integrating patch-clamp techniques with computational neuroscience models powered by large language models (LLMs), researchers have uncovered new insights into the strength and gating kinetics of $I_{Na}$ across diverse cell types [28,32,33]. These advances have also enhanced our understanding of how alterations in $I_{Na}$ influence AP firing behaviors. This review thus offers novel and important perspectives on how TEL and related agents modulate Nav channel kinetics in different cell types, ultimately shaping diverse patterns of electrical activity in excitable cells. **Table 1** outlines the intended framework of the present review.

 doi:10.20944/preprints202603.0533.v1



**Table 1.** Proposed table of contents for this review article.

| Section | Title |
|---|---|
| 1 | Introduction |
| 2 | Effect of TEL* on $I_{Na}$ identified from mHippoE-14 hippocampal neurons |
| 3 | Effect of TEL on non-activating (persistent) $I_{Na}$ recorded from mHippoE-14 hippocampal neurons |
| 4 | Effect of TEL on action current (AC) identified in mHippoE-14 neurons |
| 5 | Effect of TEL on simulated $I_{Na}$ based on Hodgkin-Huxley kinetic modeling |
| 6 | Effect of TEL on $I_{Na}$ in neurons linked to pain signaling |
| 7 | TEL-Nav1.7 channel docking prediction |
| 8 | Effect of TEL on $I_{Na}$ in HL-1 atrial cardiomyocytes |
| 9 | Simulated effect of TEL on Nav1.5 channels using a modified Markovian model derived from heart cells |
| 10 | Conclusions and future directions |

* TEL indicates telmisartan.

## 2. Effect of TEL on $I_{Na}$ Identified from mHippoE-14 Hippocampal Neurons

Previous studies have demonstrated that TEL effectively modulates the amplitude and gating behavior of $I_{Na}$ in mHippoE-14 neurons [34]. In those experiments, cells were bathed in a $Ca^{2+}$-free Tyrode's solution containing 0.5 mM $CdCl_2$ and 10 mM tetraethylammonium chloride. $CdCl_2$ was used to inhibit $Ca^2$ currents, while tetraethylammonium chloride suppresses most voltage-gated $K^+$ currents. $I_{Na}$ was then elicited by brief membrane depolarization from −80 to −10 mV, and the tail current was recorded at −50 mV. Exposure to TEL led to a pronounced elevation in the peak amplitude of $I_{Na}$, as illustrated in **Figure 2A**. However, TEL did not alter the time-to-peak of $I_{Na}$ activation in response to brief step depolarization. Additionally, TEL noticeably altered the inactivation kinetics of $I_{Na}$, resulting in a slower current decay during brief depolarizing pulse (**Figure 2B**). The inward $I_{Na}$ currents reached their maximum activation more readily, and the rate at which they decayed was significantly reduced. Upon returning to −50 mV, the relaxation phase of the current also showed marked slowing in the presence of TEL. These observations indicate that TEL enhanced $I_{Na}$ amplitude in a way that was dependent on its concentration, the functional state of Nav channels, and the temporal dynamics of current activation and inactivation [34].

Tail currents typically reflect the kinetics of Nav-channel closure (deactivation) following depolarization. In Nav channels, they are associated with how quickly channels transition from open to closed, and how this shapes the membrane potential after an AP. If deactivation is slowed, tail currents may extend the duration of inward $Na^+$ flow, subtly sustaining membrane depolarization. This residual depolarization can decrease the time needed to reach threshold for another spike, especially in neurons with high-frequency firing. Persistent tail currents can enable faster recovery from inactivation, thereby supporting more frequent APs. This can cause the membrane to linger near threshold, facilitating easier reactivation of volage-gated $Na^+$ or $Ca^{2+}$ channels [27,29,31,35].

$$\text{Closed} \underset{\beta}{\overset{\alpha}{\rightleftharpoons}} \text{Open} \underset{k_{-1}}{\overset{k_{+1}^{*}\cdot[\text{TEL}]}{\rightleftharpoons}} \text{Open}\cdot[\text{TEL}]$$

In this scheme, α and β denote the rate constants governing the opening and closing of the Nav channel. [TEL] represents the TEL concentration, while $k_{+1}^{*}$ and $k_{-1}$ denote the rate constants for forward and backward transition induced by TEL. The forward ($k_{+1}$) or backward ($k_{-1}$) rate constants, determined from the slope and y-axis intercept of the interpolated line, are 0.0344 $msec^{-1}\mu M^{-1}$ and 0.0368 $msec^{-1}$, respectively. Each point represents the mean ± SEM (n = 9-12 for each point). This figure is adapted from Lai et al. [34] and is shared under the terms of the Creative Commons Attribution (CC BY) license.

 doi:10.20944/preprints202603.0533.v1



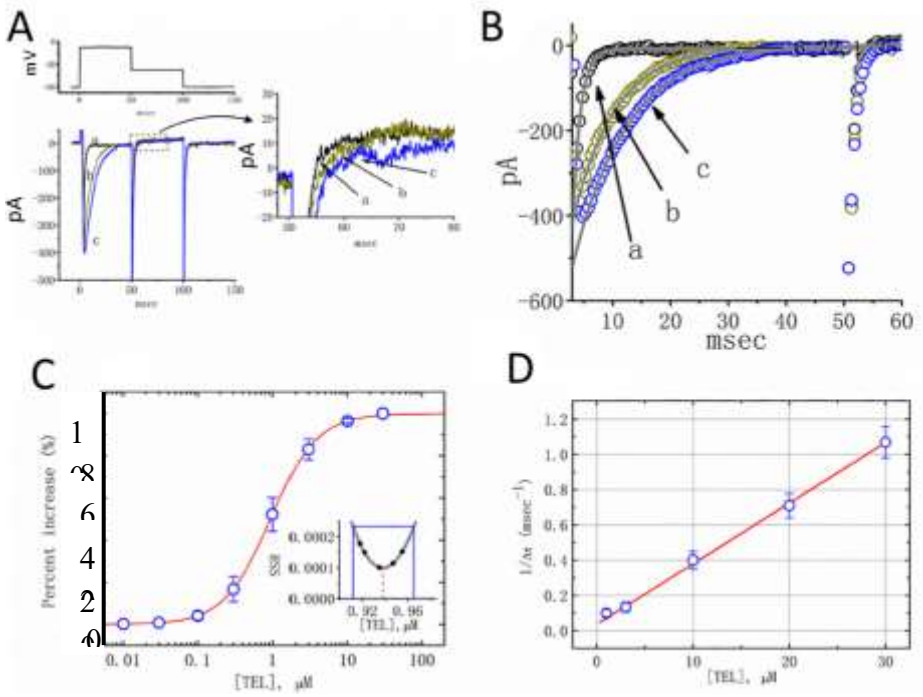


**Figure 2.** Impact of TEL on $I_{Na}$ in mHippoE-14 neurons. These experiments utilized mHippoE-14 neurons suspended in a $Ca^{2+}$-free Tyrode's solution supplemented with 0.5 mM $CdCl_2$ and 10 mM tetraethylammonium chloride. The patch pipette was filled with a $Cs^{+}$-containing solution. **(A)** Representative $I_{Na}$ traces. Traces were recorded under control conditions (a) and in the presence of 1 μM (b) and 3 μM (c) TEL. Current responses were elicited by voltage pulses (indicated in the upper part of **(A)**) depolarizing from −80 to −10 mV, followed by a repolarization step to −50 mV to measure tail (deactivating) currents (right part). The right part of **(A)** displays expanded views of these tail currents, corresponding to the segments highlighted by the dashed box. **(B)** Effects of TEL on the inactivation time course of $I_{Na}$. The inactivation time course of $I_{Na}$, both in the absence or presence of TEL, was accurately fitted using one-exponential function for control and two-exponential functions for TEL-treated conditions. Labels correspond to: a: control; b: 1 μM TEL; c: 3 μM TEL. **(C)** Concentration-dependent increase in peak $I_{Na}$ by TEL. The graph presents the percentage increases in peak $I_{Na}$ as a function of TEL concentration (mean ± SEM; n = 9-13 for each point). The smooth red line shows the best fit of a modified Hill equation to the data. From this fit, the $EC_{50}$ value for TEL-induced stimulation of $I_{Na}$ was determined to be 0.94 μM, with a Hill coefficient of 1.4. The inset in **(C)** illustrates the confidence assessment for the best-fit $EC_{50}$ value. The depicted parameter range approximates a 95% confidence interval. The blue line marks the parameter value where SSR equals 0.000234, while the broken red line indicates the $EC_{50}$ value. **(D)** Kinetic analysis of TEL's effect on $I_{Na}$ inactivation. The reciprocal of Δτ, representing the inactivation rate constant, is plotted against TEL concentration. In this analysis, Δt denotes the difference between the inactivation curve data points in the absence and presence of TEL, while Δτ is obtained by fitting a single exponential fitting to the current trajectory at each point derived from the respective Δt values. The plot of 1/Δτ versus [TEL] shows a linear relationship. The TEL's effect on $I_{Na}$ is explained by the state-dependent stimulation.

TEL's impact on peak $I_{Na}$ amplitude was concentration dependent. **Figure 2C** illustrates this relationship, showing that TEL enhanced peak $I_{Na}$ as its concentration increased. The estimated half-maximal effective concentration ($EC_{50}$) for this stimulation was 0.94 ± 004 μM. At 30 μM, TEL achieved its maximal effect, significantly increasing the peak $I_{Na}$ amplitude in mHippoE-14 neurons [34]. The inset of **Figure 2C** displays the sum of squared residuals (SSR) plot, where a horizontal line at SSR = 0.000234 indicates the two $EC_{50}$ values used in the analysis. The 95% confidence interval for the $EC_{50}$ was determined to be 0.912 to 0.965 μM, respectively. The distinct $EC_{50}$ value for TEL-stimulated $I_{Na}$ was clearly identifiable, which is supported by the steep slope observed on both sides of the minimal sum of squared residuals (SSR) [34,36]. These data demonstrate that TEL stimulates the $I_{Na}$ amplitude in these cells.

 doi:10.20944/preprints202603.0533.v1



Increasing TEL concentrations not only augmented the peak $I_{Na}$ amplitude but also significantly slowed its inactivation. Analysis using a first-order binding reaction (**Figure 2D**) yielded forward ($k_{+1}$) and backward ($k_{-1}$) rate constants of 0.0344 $msec^{-1}\mu M^{-1}$ and 0.0365 $msec^{-1}$, respectively [34]. From these constants, the apparent dissociation constant ($K_D$), defined as $k_{-1}$ / $k_{+1}$, for TEL binding to Nav channels was calculated to be 1.04 μM. This $K_D$ value closely matches the $EC_{50}$ for TEL-induced peak $I_{Na}$ stimulation observed in the concentration-response curve (**Figure 2C**).

## 3. Effect of TEL on Non-Activating (Persistent) $I_{Na}$ Recorded from mHippoE-14 Hippocampal Neurons

The non-inactivating or persistent $I_{Na}$ ($I_{Na(NI)}$) is a known feature of neurons and neuroendocrine cells [28,30,37,38]. This current has been implicated in conditions such as epilepsy and neuropathic pain [27,28,35]. Previous studies investigated whether TEL perturbs the amplitude of $I_{Na(NI)}$ in these cells when stimulated by a 2-sec ramp pulse [34]. During the whole-cell current recording, when the mHippoE-14 neuron was voltage-clamped at −50 mV, a long-lasting ramp pulse from −100 to +100 mV was applied. The results demonstrated that 3 μM TEL enhanced $I_{Na(NI)}$ when elicited by a long ramp pulse (**Figure 3A**). Subsequent application of ranolazine (Ran, 10 μM) or eugenol (EUG, 10 μM), both known $I_{Na(NI)}$ inhibitors [39,40], attenuated the TEL-induced stimulation of $I_{Na(NI)}$ evoked during the long ramp pulse (**Figure 3B**).

While Ran and EUG significantly reverse the TEL-induced increase in $I_{Na(NI)}$ amplitude, the absolute change remains modest. This suggests that the primary modulatory effects of TEL, and its reversal by Ran or EUG, may extend beyond $I_{Na(NI)}$ channels. The small magnitude of change in $I_{Na(NI)}$ implies that non-$I_{Na(NI)}$ components—such as residual tetrodotoxin-resistant currents or altered channel gating properties in other Nav channel population—may contribute substantially to the overall current modulation. The potential involvement of other channel subtypes or mechanisms in the observed pharmacological effects needs to be further delineated.

Existing studies on Ran and EUG refer to different cell types, and caution against direct extrapolation to hippocampal neurons. In terms of Ran's proposed binding site on Nav channels, the lack of evidence for competitive binding between TEL and ranolazine is shown. This thus remains a hypothesis needing further study. Additionally, further addition of angiotensin II (200 nM) or chlorotoxin (1 μM), a known $Cl^-$ channel blocker, had no effects on TEL-induced increases in $I_{Na(NI)}$. These findings suggest that TEL's effect on $I_{Na(NI)}$ in these cells is independent of either ACE inhibition or $Cl^-$ channel modulation [34,41].

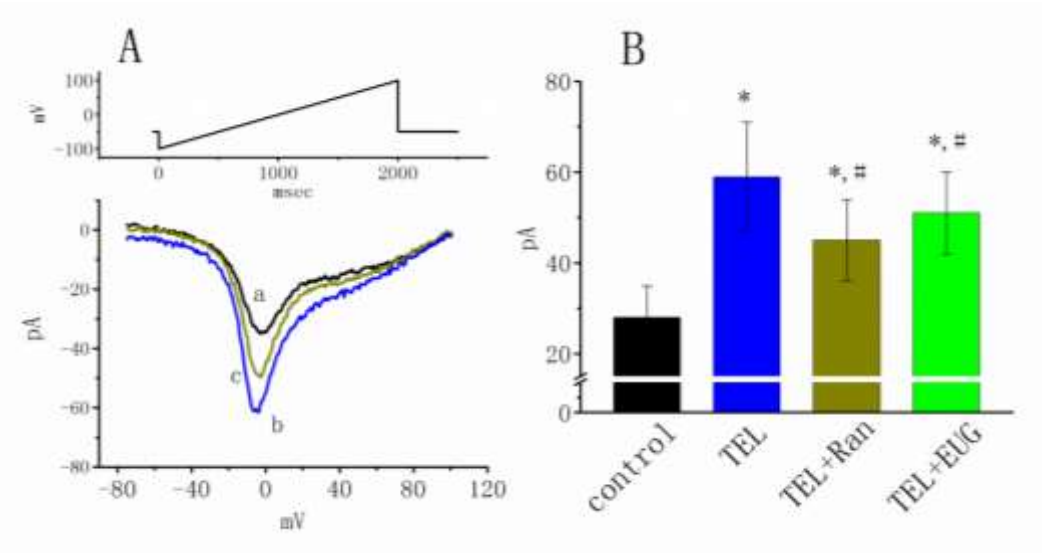


**Figure 3.** Effects of TEL, TEL in combination with ranolazine (Ran), or TEL in combination with eugenol (EUG) on non-inactivating $I_{Na}$ ($I_{Na(NI)}$) in mHippoE-14 hippocampal neurons. In these experiments, each cell was

 doi:10.20944/preprints202603.0533.v1



voltage-clamped at −50 mV. A 2-sec long ramp pulse from −100 to +100 mV (as shown in the top panel of **(A)**), was applied at a rate of 0.05 Hz. **(A)** Representative $I_{Na(NI)}$ traces. Traces were evoked by the ramp pulse and recorded under control conditions, after application of TEL, and with TEL combined with Ran. Labels are: a: control; b: TEL (3 μM); c: TEL (3 μM) plus Ran (10 μM). **(B)** Summary of $I_{Na}$ peak amplitude data. This bar graph illustrates the effects of TEL (3 μM), TEL (3 μM) combined with Ran (10 μM), or Tel (3 μM) combined with EUG (10 μM) on the peak amplitude of $I_{Na(NI)}$ (mean ± SEM; n = 10-12 for each bar). *Significantly different from control ($p < 0.05$) and #significantly different from the TEL (3 μM) alone group ($p < 0.05$). Notably, both Ran and EUG significantly reversed the TEL-induced increase in $I_{Na(NI)}$ amplitude in these cells. This figure is adapted from Lai et al. [34] and is shared under the terms of the Creative Commons Attribution (CC BY) license.

## 4. Effect of TEL on Action Current (AC) Identified in mHippoE-14 Neurons

As changes in $I_{Na(NI)}$ strength are known to affect neuronal AP emergence [37,38], we sought to determine if TEL could perturb the transient depolarization involved in initiating excitation in mHippoE-14 neuron was determined (**Figure 4**). In these experiments, with the cell held at −100 mV, repetitive triangular voltage pulses, each 800 msec in duration, were applied. The resulting current traces obtained from this voltage-clamp protocol are shown in **Figure 4A**. Notably, the AC consistently occurs during the upsloping phase of the ramp, but not during the downsloping phase.

Concurrently, activity of large-conductance $Ca^{2+}$-activated $K^+$ ($BK_{Ca}$) channels—evident as random downward deflections—was observed at −100 mV relative to the resting potential, suggesting the presence of $BK_{Ca}$-channel activity in these cells. This activity is effectively suppressed by paxilline, confirming the involvement of $BK_{Ca}$ channels in these cells. However, the TEL exposure did not alter the activity of $BK_{Ca}$ channels under this experimental condition, suggesting that TEL did not modulate $BK_{Ca}$-channel activity directly [34,42].

Furthermore, when mHippoE-14 cells were exposed to TEL, the latency of AC generation in response to the triangular voltage ramps significantly shortened [34]. Subsequent addition of Ran (10 μM) was observed to reverse this TEL-mediated reduction in the latency of AC generation (**Figure 4B**). This TEL-mediated shortening of AC generation latency is strongly associated with its effectiveness in stimulating $I_{Na(NI)}$.

This review highlights the effects of TEL on $I_{Na}$ observed in various neuronal models and excitable tissues, including cardiac cells and sensory neurons, where relevant data are available. Importantly, no studies have yet confirmed direct binding of TEL on $Na_V$ channels, and existing evidence does not rule out the possibility of indirect mechanisms.

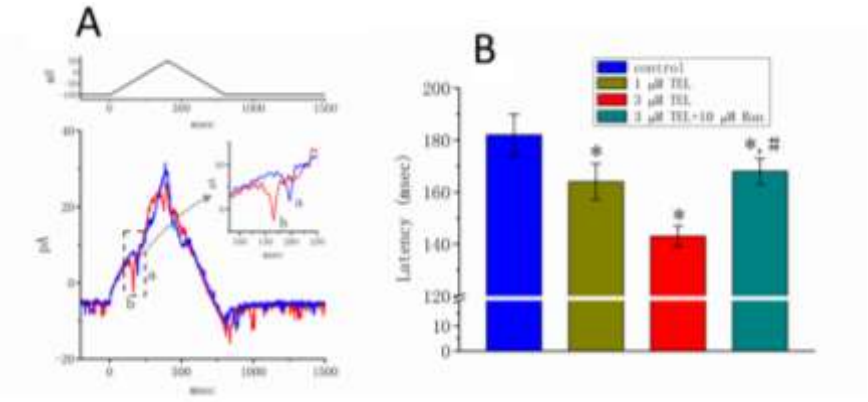


**Figure 4.** Effect of TEL on action currents (ACs) elicited by triangular voltage ramp. In these experiments, cell-attached current recordings were performed on cells bathed in normal Tyrode's solution containing 1.8 mM $CaCl_2$. The holding potential was maintained at −100 mV, resulting in a membrane potential of approximately +30 mV relative to the cell's resting potential during cell-attached recordings. Triangular ramp pulses, each 800 msec in duration (indicated in the upper part of panel **(A)**), were delivered at a rate of 0.05 Hz. **(A)** Representative AC traces. Current traces evoked by the triangular voltage ramp were obtained under control conditions (a) and

 doi:10.20944/preprints202603.0533.v1



during cell exposure to 3 μM TEL (b). The inset provides an enlarged view of an action current (AC), corresponding to the occurrence of an AP (dashed box), which manifests as a brief downward deflecting spike. Notably, these spikes appear exclusively during the upsloping phase of the ramp, but not during the downsloping phase. **(B)** Latency of AC generation. This bar graph summaries the effects of TEL and TEL combined with Ran on the latency of AC generation elicited by triangular voltage ramps (mean ± SEM; n = 6-9 for each bar). The latency is defined as the time delay between the initiation of the ramp pulse and the onset of AC. *Significantly different from control group ($p < 0.05$) and #significantly different from 3 μM TEL-alone group ($p < 0.05$). This figure is adapted from Lai et al. [34] and is shared under the terms of the Creative Commons Attribution (CC BY) license.

## 5. Effect of TEL on Simulated $I_{Na}$ Based on Hodgkin-Huxley Kinetic Modeling

To investigate TEL's effects on neuronal $I_{Na}$ amplitude and kinetics, a Hodgkin-Huxley-based model was computationally developed in a previous study [32,38,43]. This model, designed to mimic TEL's impact on neuronal function, incorporated a stepwise change in the '*h*' inactivation gating variable parameter to predict membrane potential alterations.

The inactivation parameter of $I_{Na}$ used for mimicking the effect of TEL on this current is formulated by $h = (\phi \times \alpha_h) / (\alpha_h + \beta_h)$, where $h$ is inactivation gating variable, $\alpha_h$ and $\beta_h$ are the rate constants for inactivation gating variable, and the parameter $\phi$ represents the magnitude of Nav-channel inactivation [43].

Changes in membrane potential ($V$) at different $\phi$ values were further determined. As shown in **Figure 5A**, when the $\phi$ value was set at 1.0 and the value of $Na^+$-current conductance arbitrarily fixed at 190 mS/cm$^2$, the membrane potential ($V$) initially exhibited slight fluctuations before reaching an equilibrium state over time. The corresponding trajectories of the gating variables $m$, $h$, and $n$ are presented in **Figure 5B**. These results indicate that the modeled cell's electrical behavior stabilizes into an equilibrium state, likely because the $Na^+$-current conductance (190 mS/cm$^2$) is below the system's bifurcation point (212.6 mS/cm$^2$).

Notably, in this system, increasing the $\phi$ value slows the time course of Nav channel inactivation caused by membrane depolarization, while also increasing current amplitude. When $\phi$ was increased to 2.0 to mimic a slowed $I_{Na}$ inactivation, the system became unstable, leading to a periodical change in V (**Figure 5C**). Consequently, repetitive AP firing emerged (**Figure 5C**), and the trajectories of $m$, $h$, and $n$ eventually formed limit cycles (**Figure 5D**). Under this condition, the modeled cell's electrical activity entered a periodic, unstable state at a specific frequency. Therefore, a stepwise increase in the $\phi$ value, which mimics the stimulatory effect of TEL on $I_{Na}$, effectively increases the firing tendency of this model [43].

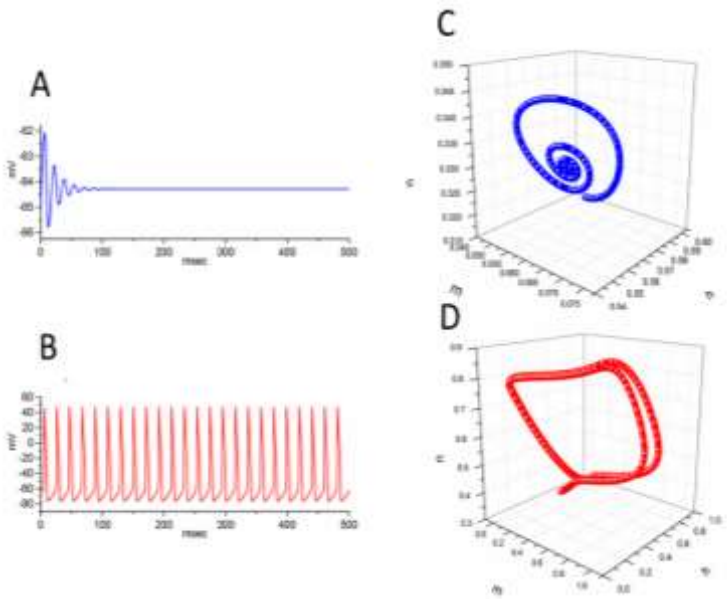

 doi:10.20944/preprints202603.0533.v1



**Figure 5.** Simulated membrane potential dynamics and gating variable trajectories. **(A)** and **(C)** show blue traces illustrating time-dependent changes in membrane potential and three-dimensional trajectories of the gating variables *m*, *n*, and *h*, respectively, based on Hodgkin-Huxley kinetics with an $I_{Na}$ conductance of 190 mS/cm$^2$. All other simulation parameters were maintained at their default setting as previously described [32,33,38,43]. The inactivation gating variable h was assigned a f value of 1.0 in panels **A** and **C** (blue traces), and 2.0 in panels **B** and **D** (red traces). Elevating the $\phi$ value slows inactivation of $I_{Na}$, thereby altering neuronal excitability pattern. This figure is adapted from Chang et al. [43] and is shared under the terms of the Creative Commons Attribution (CC BY) license.

## 6. Effect of TEL on $I_{Na}$ in Neurons Linked to Pain Signaling

Another study also demonstrated that TEL increased $I_{Na}$ amplitude and slowed its inactivation time course in cultured dorsal root ganglion (DRG) neurons [28]. A subsequent addition of KB-R7943, known to suppress the activity of $Na^+$-$Ca^{2+}$ exchanging process [44], could reverse TEL-simulated $I_{Na}$ [28,45]. KB-R7943 was reported to play a role in shaping intracellular ionic dynamics under pathological or experimentally manipulated conditions. However, recent findings demonstrated that KB-R7943 effectively suppressed $I_{Na}$ [28,45] and that TEL-stimulated $I_{Na}$ could be attenuated by the subsequent addition of KB-R7943, suggesting KB-R7943 might be an inhibitor of $I_{Na}$.

In this study by Huang et al., 2024 [28], the investigators also employed a theoretical model of AP firing in parvalbumin-expressing neurons (PVINs), which was adapted from a previous study by Ma et al. [46]. Parvalbumin (PV) is a calcium-binding protein that marks a subset of fast-spiking interneurons, and PVINs in the hippocampus were reported to influence contextual fear, memory and cognitive flexibility [47]. The model's foundation lies in the biophysical properties of PVINs found within the dorsal horn of the spinal cord [46]. The XPPAUT simulation package was utilized to conduct analyses related to linear stability and bifurcation [28,33,48,49].

Bifurcation analysis was employed to investigate alterations in the modeled neuron's steady-state membrane potential in response to variations in the applied current (Iapp). A bifurcation diagraph graphically represents the long-term behavior of a dynamical system as a parameter is systematically changed [32,33,48]. As shown in **Figure 6**, these simulations treated Iapp as a variable while maintaining all other parameters at their default values [28].

With the constant '$\phi$' value set to 1, **Figure 6** illustrates the bifurcation diagram, detailing the correlation between Iapp and the resulting membrane potential changes. Two critical Iapp values, representing subcritical and supercritical Hopf bifurcation points, were identified. Specifically, these points at $\phi = 1$ were found to be 88 and 177 pA, respectively. Within this range of Iapp values, a stable limit cycle emerged, forming a closed trajectory indicative of subthreshold oscillation (SO) in the modeled neuron, consistent with previous demonstrations [28,32,50]. The corresponding membrane potential fluctuations were observed to be between −39.3 and −36.2 mV. The model thus exhibits stability when Iapp is below the subcritical point or above the supercritical point. However, self-sustained periodic oscillations, or SOs, occur when Iapp falls within the range between these two Hopf bifurcation points (**Figure 6A**).

When the $\phi$ value in the $\beta_h$ inactivation process of the *h* inactivation variable was reduced to 0.8, while the $Na^+$ current conductance remained fixed at 300 nS, a significant change was observed in the bifurcation diagram. This adjustment effectively simulated a slower inactivation time course for the $I_{Na}$ (**Figure 6B**). In contrast to the system shown in **Figure 6**, a decrease in the $\phi$ value in this system resulted in a delayed inactivation of $I_{Na}$ elicited by step depolarization. Under these altered conditions, the system exhibited two distinct types of periodical solutions were observed [28]. Specificially, the subcritical and supercritical points, which mark the initiation of the pre-existing SO, shifted to 95 and 367 pA, respectively. Furthermore, within the Iapp range of 52 to 95 pA, somatic spike (SS), or somatic AP firing, was observed. In this SS domain, the membrane potential varied between −40 and +15 mV. Notably, as depicted in **Figure 6B,** when the SO domain overlapped with the SS domain, the system demonstrated SS/SO bistability for Iapp amplitudes between 79 and 118 pA [28]. It is important to note that neurons in the dorsal horn of the spinal cord, including PVINs,

 doi:10.20944/preprints202603.0533.v1



could display greater heterogeneity compared to DRG neurons. The observed effects of TEL may have significant implications for neural biological activity. The regulation of ion channels in the cell membrane, such as the Nav channel, is likely a crucial underlying mechanism for pain-related signaling [28,34,51,52].

Notably, **Figure 6** illustrates a simulated bifurcation analysis, which is inherently a computational exploration of dynamical system behavior under varying parameter conditions. While the specific bifurcation patterns shown in this figure have not yet been directly validated through electrophysiological experiments, our modeling framework builds upon established biophysical principles. The simulation results provide testable prediction regarding membrane excitability transitions and ionic conductance thresholds, which can guide future experimental designs aimed at validating the model's dynamic regimes. This figure represents a theoretical construct intended to inform and inspire subsequent empirical investigations [28].

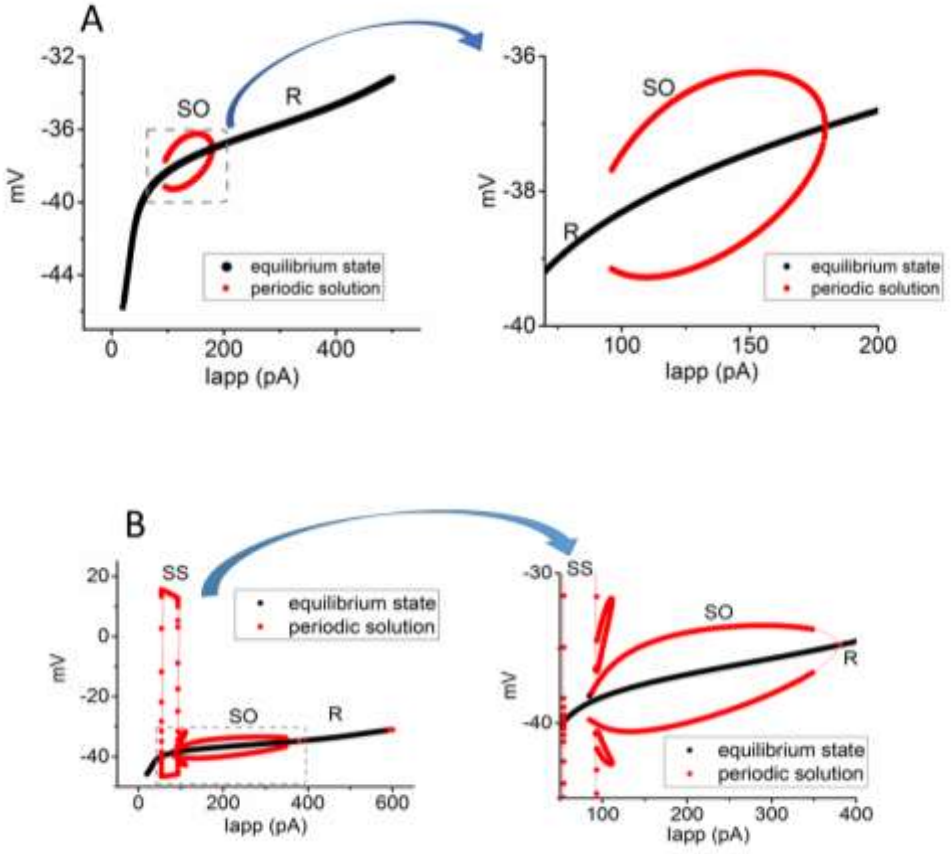


**Figure 6.** Bifurcation diagram of membrane potential dynamics in a PVIN-based neuronal model. This diagram depicts the bifurcation relationship between applied current (Iapp) and changes in membrane potential in a computational model, reflecting the biophysical properties of PVINs located in the dorsal horn of the spinal cord. Simulations were carried out using default parameters as described in Huang et al. [28] with the inactivation gating parameter $\phi$ value set to 1.0 **(A)** and 0.8 **(B)**. In **(A)**, two dynamic regimes were identified: a resting, steady-state equilibrium (R, shown in black) and an unstable, periodic trajectory indicative of subthreshold oscillation (SO, shown in red). In **(B)**, beyoind the equilibrium or resting state (R, in black), two distinct periodic solutions emerged (indicated in red), including somatic spike (SS) within the Iapp range of 52–97 pA and SO across 85–381 pA. The enlarged subpanels on the right side of **(A)** and **(B)** highlight details of the boxed region on the left. This figure is adapted from Huang et al. [28] and is licensed under the Creative Commons Attribution (CC BY) license.

 doi:10.20944/preprints202603.0533.v1



## 7. Docking Predictions for TEL-Nav1.7 Channel and TEL-PPAR-γ

A previous study identified a distinct, high-affinity interaction between TEL and the AT1 receptor [53]. Building upon this, we conducted a detailed analysis of the atomic interactions between the Nav1.7-channel protein and TEL using PyRx software (available at http://pyrx.source-forge.io/, accessed on 6 March 2026). The Nav channel, encoded by the *SCN9A* gene, is predominantly expressed in the peripheral nervous system and plays a crucial role in pain signaling.

**Figure 7** illustrates the predicted docking sites of the TEL molecule. During the docking simulation with the Nav1.7 channel, TEL formed hydrogen bonds with residues Asn31(L) and Tyr103(L), at distances of 3.03 and 3.26 Å, respectively. Additionally, TEL exhibited hydrophobic interactions with several other residues, including Ser30(L), Glu882(C), Trp883(B), Ser902(B), Ser902(C), Met905(A), Met905(B), Gly906(B), Arg909(B), and Glu913(B). The hydrophobic effect is the driving force that brings nonpolar molecules together in an aqueous environment, primarily due to entropic considerations of the water molecules. These findings collectively suggest a strong binding affinity between TEL and the amino-acid residues of the Nav1.7 channel, with an estimated interaction energy of –7.6 kcal/mol.

The carboxylic acid group in the TEL molecule contributes to hydrogen bonding and enhances water solubility, while the benzimidazole and biphenyl moieties engage in hydrophobic interactions with the channel, establishing lipophilic parts. TEL can be described as having amphipathic properties, though not as strongly as classic surfactants or bile acids. It is possible that the specific domain (e.g., domain IV voltage-sensing region) of hNav is associated with TEL docking. Alternatively, an earlier report identified the binding site of TEL on Nav1.5 channels near Ser571 [54], which appears to differ from its predicted docking site on Nav1.7 channels shown here. Nevertheless, this predicted interaction between TEL and the Nav1.7 channel raises important questions about how TEL might influence the magnitude and gating kinetics of $I_{Na}$ [28,34,51,52].

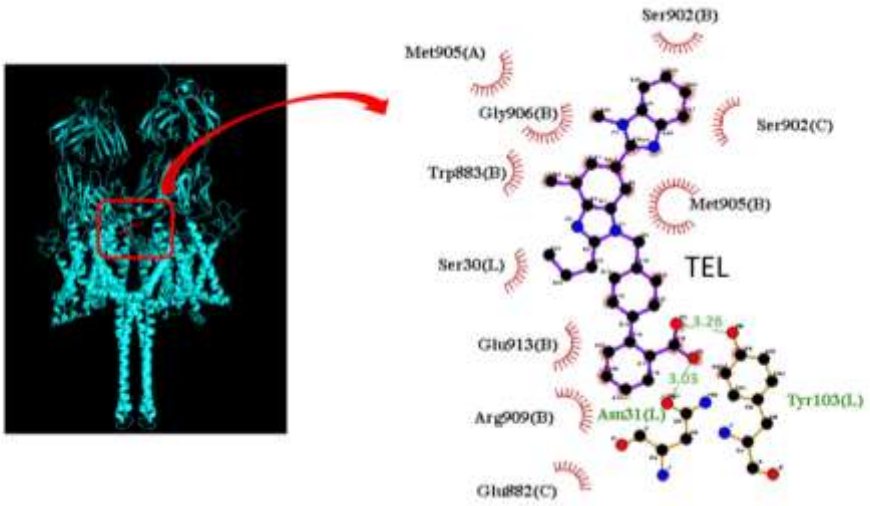


**Figure 7.** Predicted docking interaction between telmisartan (TEL) and the human NaV1.7 channel. This figure illustrates the molecular docking prediction of TEL with the NaV channel. The protein structure of NaV1.7 was obtained from the Protein Data Bank (PDB: 6N4Q), while the 3-dimensional chemical structure of TEL was sourced from PubChem (CID: 65999). The left panel was generated using PyMOL (https://www.pymol.org/, accessed on 6 March 2026) or BIOVIA (https://www.3ds.com/products/biovia/discovery-studio/visualization, accessed on 28 July 2025). This snapshot—highlighted by a red box—depicts the docked TEL molecule within the NaV1.7 channel. Key interactions, including hydrophobic contacts and hydrogen bond formation, are indicated. In the right panel, the molecular interactions were rendered using LigPlot+ (http://www.ebi.ac.uk/thornton-sevLIGPLOT; accessed on 6 March 2026). The structure enclosed by the small red box shows the TEL molecule docked within the NaV channel. Note that the red arcs, with radial spokes

 doi:10.20944/preprints202603.0533.v1



pointing toward the TEL molecule, indicate hydrophobic contacts. The green dashed lines indicate hydrogen bonds, with measured bond distances of 3.03 and 3.26 Å. The letter in parenthesis following each residue number indicates the corresponding chain identifier in this and the following figures.

Because TEL has been reported to exert agonistic interactions with human PPAR-γ, we further investigated the potential molecular interactions between telmisartan and the PPAR-γ structure (**Figure 8**). The three-dimensional structure of PPAR-γ was obtained from the Protein Data Bank (PDB ID: 4YT1), and the TEL structure was retrieved from PubChem (CID: 6599). The predicted docking results revealed that multiple amino acid residues form hydrophobic contacts with the PPAR-γ structure, including Phe282(B), Ser289(B), Val290(B), Val293(B), Gln294(B), His323(B), His449(B), Leu453(B), Ile472(B), Lys474(B), and Val450(B). In addition, telmisartan forms hydrogen bonds with Gln286(B) and Lys319(B), both at a distance of 3.03 Å. The docking interaction exhibited a binding affinity of −8.7 kcal/mol. These findings indicate that telmisartan demonstrates a strong docking interaction with PPAR-γ.

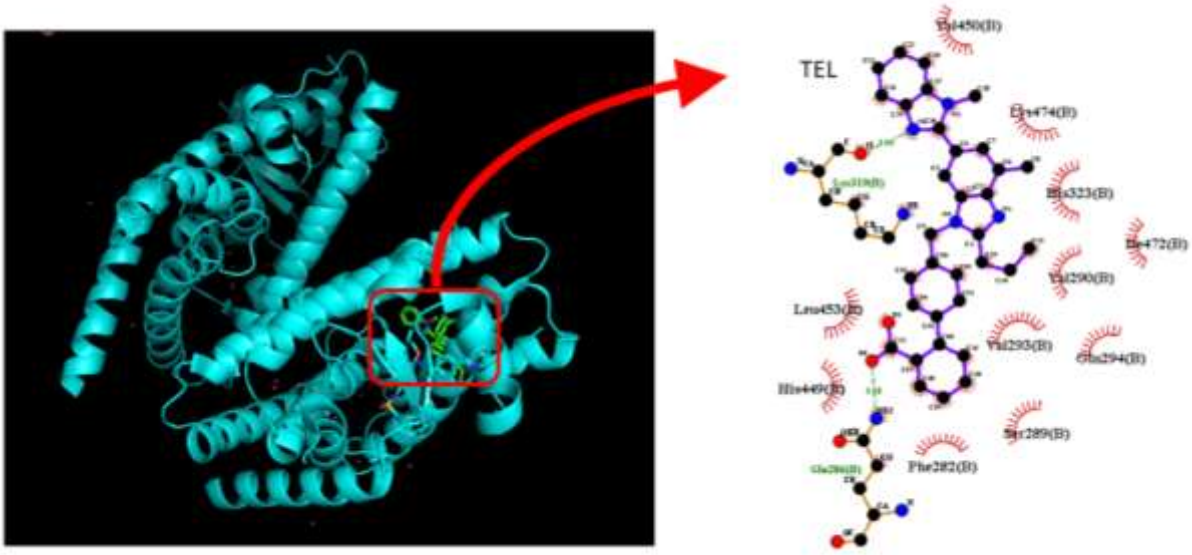


**Figure 8.** Docking interaction between telmisartan (TEL) and PPAR-γ. The structure of PPAR-γ was obtained from the Protein Data Bank (PDB ID: 4YT1), and the three-dimensional chemical structure of TEL was retrieved from PubChem (CID: 6599). The left panel shows the docking result generated by PyRx software after autodocking, with the red box indicating the docking site of the TEL molecule within the PPAR-γ protein. The right panel illustrates the atomic interactions as analyzed and visualized using LigPlot+. The structure within the small red box represents the TEL molecule docked into the PPAR-γ structure. The red arcs with radial spokes directed toward the TEL molecule denote hydrophobic interactions. The green dashed lines indicate hydrogen bonds, both with measured bond distance of 3.03 Å.

## 8. Effect of TEL on $I_{Na}$ in HL-1 Atrial Cardiomyocytes

A prior study showed that at therapeutic concentrations, a compound called TEL significantly and differentially enhanced both the peak and late components of $I_{Na}$ in a concentration-dependent manner [55]. In HL-1 cardiomyocytes, the $EC_{50}$ values for this stimulatory effect on peak and late $I_{Na}$ were determined to be 0.2 and 1.2 μM, respectively. Furthermore, TEL was found to accelerate the recovery from $I_{Na}$ inactivation and increase the inactivation time constant of late $I_{Na}$ found in these cells. In addition, TEL similarly augmented peak $I_{Na}$ and slowed its current inactivation in coronary smooth muscle cells. Conversely, TEL also suppressed the magnitude of *erg*-mediated $K^+$ current in HL-1 cells [55]. The results from these in vitro experiments suggest that TEL has the potential to

 doi:10.20944/preprints202603.0533.v1



increase the membrane excitability of heart cells in vivo by preferentially interacting with the inactivated states of Nav1.5 channels.

## 9. Simulated Effect of TEL on Nav1.5 Channels Using a Modified Markovian Model Derived from Heart Cells

To further clarify the ionic mechanisms underlying TEL's stimulatory actions, a modified Markovian model of $I_{Na}$ in cardiac cells was employed for analysis. This model is particularly relevant as the predominant Nav channel isoform in these cells, responsible for $I_{Na}$, is Nav1.5, which is encoded by the *SCN5A* gene [56]. A Markovian model for simulating Nav channels is a mathematical framework that describes the stochastic (random) transitions between various functional states of the Nav channel—such as closed, open, and inactivated—over time. The Markovian model used to simulate $I_{Na}$ in cardiac cells, as illustrated in **Figure 9A**, was based on the original formulation by Clancy and Rudy [57], with their paper providing the detailed parameters. This model fundamentally comprises three closed states, one open state, one fast inactivation state, two closed-inactivation states, and two intermediate inactivated states [56,57].

As illustrated in **Figure 9B**, the simulated stimulatory effect of TEL on $I_{Na}$ in cardiac cells remarkably mirrored the experimental observations [43,55]. These results indicated that TEL's stimulatory action at concentrations of 10 and 30 μM could be replicated in the model by reducing $\alpha_2$ (i.e., transitional rate from fast inactivation (IF) to open (O) state) to 19 and 10 $msec^{-1}$ from a control vale of 29.6 $msec^{-1}$. This effectively means that TEL slowed the progression toward the activated state by 36 and 66% at 10 and 30 μM TEL, respectively. Consequently, these model findings are in excellent agreement with experimental data, which showed that exposing cells to TEL (10 and 30 μM) led to increased $I_{Na}$ amplitudes in response to step depolarization, alongside an increase in the current's inactivation time constant [43,55]. It is therefore anticipated that the influence of TEL on $\alpha_2$ transition rate affects open-channel dynamics, highlighting the possibility of cell-type specific effects on inactivation kinetics.

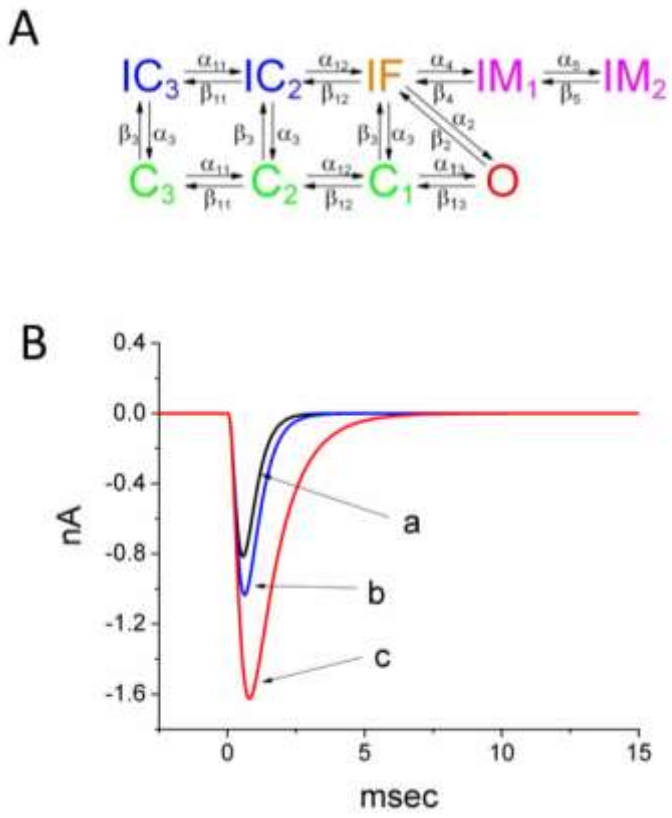

 doi:10.20944/preprints202603.0533.v1



**Figure 9.** Simulation of TEL-induced modulation of $I_{Na}$ in cardiac cells. **(A)** Markovian model depicting $I_{Na}$ dynamics, adapted from Clancy and Rudy [57]. The model equations are accessible via ModelDB (http://senselab.med.yale.edu/senselab/modeldb; accessed on 6 March 2026) and were solved using the XPPAUT software package. Default parameter values under control conditions were adopted as specified by Clancy and Rudy [57]. In **(A)**, states are indicated as follows: C: Closed state; O: Open state; IF: Fast inactivation state; IC: Closed-inactivation state; IM: Intermediate inactivation state. In **(B)**, the simulated $I_{Na}$ traces in response to depolarization from −80 to −10 mV are illustrated. Modifying the value of $\alpha_2$ from its control value of 20.6 $msec^{-1}$ (a) to 19 $msec^{-1}$ (b) and 10 $msec^{-1}$ (c) resulted in an increased peak current amplitude and a slower inactivation time course.Traces (b) and (c) approximate the effects of 10 and 30 μM TEL, respectively.

## 10. Conclusions and Future Directions

This review article explains that TEL exerts a stimulatory effect on $I_{Na}$ in various types of electrically excitable cells observed in culture or *in vitro*, and also slows down the inactivation process of this current, with a relatively rapid onset of action [34,40,41,43,51,52,55]. However, under in vivo conditions, the primary actions of TEL include: (1) high-affinity inhibition of angiotensin II binding to its AT1 receptors, (2) stimulation of $I_{Na}$, and (3) activation of PPAR-γ, as illustrated in **Figure 10**. The first effect requires the presence of angiotensin II, while the third effect depends on TEL entering the cytoplasm, and even the nucleus, to exert its action. The latter may require TEL to enter the cell, and it takes a longer duration to take effect [6]. Future investigations using heterologous expression platforms or structural modeling would be important next steps to elucidate TEL's mechanism of action on Nav channels. To establishing direct TEL-Nav interactions remains to be further investigated.

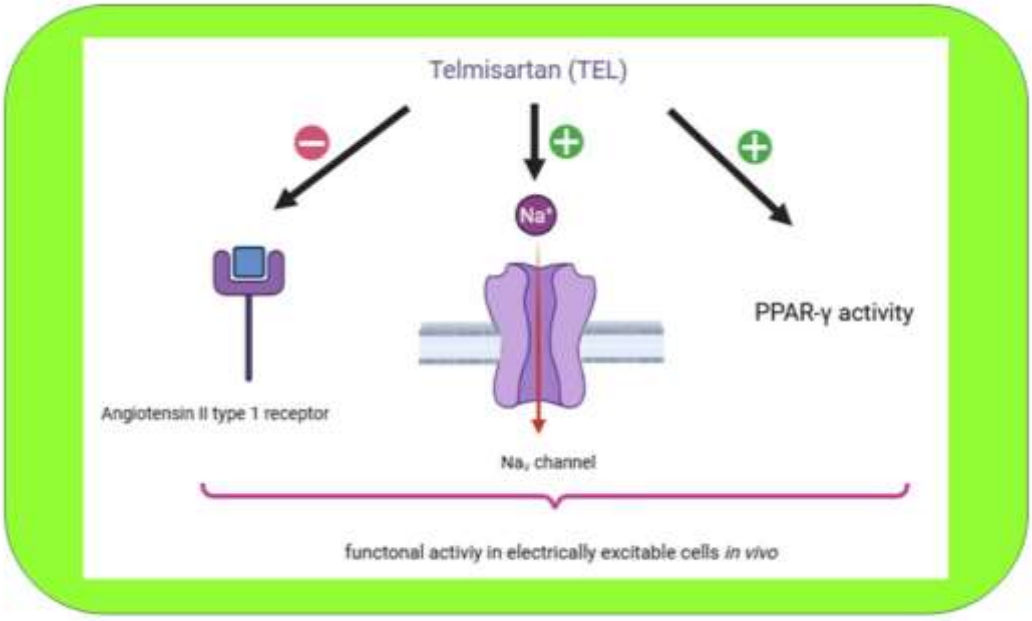


**Figure 10.** Schematic illustration of the three primary effects of TEL on electrically excitable cells in vivo: (1) blockade of angiotensin II type 1 (AT1) receptors, (2) activation of $I_{Na}$ and slowing of current inactivation, and (3) agonistic effect on the activity of peroxisome proliferator-activated receptors-γ (PPAR-γ). The '+' symbol denotes a stimulatory or an agonistic action, whereas the '−' symbol signifies inhibition via AT1 receptor blockade. The downward-pointing red arrow in the center indicates that when the Nav channel opens, $Na^+$ ions flow into the cell from the extracellular space with high specificity and exclusivity, driven by their electrochemical gradient.

 doi:10.20944/preprints202603.0533.v1



In in vivo experiments involving the central nervous system, aside from electrically excitable cells such as neurons, non-excitable cell types—including astrocytes, microglia, oligodendrocytes, and vascular endothelial cells—are more significantly affected by TEL through its PPAR-γ agonism and AT1 receptor blockade [5]. This is particularly relevant because most of these non-excitable cells lack functional expression of Nav-channels. However, within the central nervous system, there is even greater variability in angiotensin II concentrations or angiotensin-converting enzyme (ACE) activity among different nuclei [5]. Alternatively, a recent report has shown that TEL exerts antiproliferative and apoptotic effects on glioma [58,59]. Glioma cells have also been found to express Nav channels [60]. Therefore, it warrants further investigation whether the growth-inhibitory effects of TEL on glioma are associated with its stimulation of $I_{Na}$.

Notably, the antihypertensive effect of TEL is primarily due to its blockade of AT1 receptors [1–3]. However, if TEL exerts its vascular effects through competitive inhibition of angiotensin II binding to AT1 receptors, its potency or efficacy may be influenced by the extracellular or plasma concentration of angiotensin II, the ACE activity, or both [4]. On the other hand, the vascular effects of $I_{Na}$ activators may not be very pronounced, although TEL was reported to augment peak $I_{Na}$ in coronary smooth muscle cells [55]. Moreover, in clinical practice, some combination drugs—such as Co-Midis® and Twynsta® (containing telmisartan and amlodipine), or Zinipress® and Telnitaz® (containing telmisartan and azelnidipine)—also exert $Ca^{2+}$ channel-blocking effects, which contribute significantly to their overall antihypertensive efficacy [61,62]. However, the combination of telmisartan and dapagliflozin [63] presents a somewhat unconventional pharmacological profile, as gliflozin-class compounds like dapagliflozin are known to block $I_{Na}$ and $I_{Na(NI)}$ [64]. Furthermore, distinguishing TEL's effects on angiotensin II receptors versus ion channels is critical to understanding its diverse physiological outcomes.

Previous research indicates varying plasma concentration of TEL following administration. According to a previous report [65], a single oral dose of TEL at 8 mg/kg in rats resulted in a peak plasma concentration of approximately 700 ng/mL (≈ 1.36 μM) within 10 hours. Another study reported that in humans, a single 40 mg dose of TEL achieved peak plasma concentrations of approximately 44.7 ng/ml (0.087 μM) after oral administration and 1196 ng/ml (2.32 μM) following intravenous administration [66]. When treating hypertension, the usual starting oral dose for treating hypertension is 40 mg once daily. For cardiovascular risk reduction, the recommended dose is 80 mg once daily. Taken together, these findings suggest that TEL can attain plasma concentrations that fall within the pharmacologically relevant range necessary for $I_{Na}$ activation [65–67]. Given their pronounced lipophilicity and proven ability to cross the blood-brain barrier [4,5], TEL—along with other structurally related sartan-type compounds such as azilsartan, candesartan, losartan, and valsartan—may exert modulatory effects on neurons and neuroendocrine cells *in vivo*. One plausible mechanism for these central nervous system effects involves their stimulatory influence on Nav channels.

The high plasma TEL concentrations (~2 μM) reported following intravenous administration are transient and not representative of routine clinical use, where oral administration is standard. Therefore, while these pharmacokinetic studies offer insight into TEL's dose-dependent plasma levels, it needs to be noted that the concentrations sufficient to activate $I_{Na}$ are more readily achieved via intravenous administration, which is not commonly employed in clinical settings. Furthermore, to our knowledge, no studies have reported neuronal side effects arising from TEL administration in humans, supporting the notion that the observed $I_{Na}$ modulation is of pharmacological interest but not yet of established clinical significance.

It is important to note that pyrethroids—such as deltamethrin or tefluthrin—are a group of synthetic insecticide that also exert significant stimulatory effects on $I_{Na}$ in various types of excitable cells [40,68,69]. However, unlike TEL, exposure to these compounds is associated with impairments in cognitive function [22,70–72]. A recent study showed that TEL attenuated behavioral alterations and modulated cytokine levels, although it might impair spatial working memory in a specific murine model [73]. In addition, a population-based analysis reported that, among patients with

 doi:10.20944/preprints202603.0533.v1



hypertension, TEL was associated with a lower risk of overall dementia and stroke compared with other renin-angiotensin system (RAS) inhibitors in patients with hypertension [74]. Therefore, the impact of various $I_{Na}$ activators on brain cognitive functions or memory consolidation still requires further in-depth investigation.

**Author Contributions:** Writing—review & editing, Supervision, Validation, Investigation, Dara curation, Conceptualization—S.-N.W., Investigation, Data curation, Funding acquisition, Conceptualization, Project administration—R.L., Investigation, Data curation, Funding acquisition, Conceptualization, Project administration—V.R., Investigation, Data curation, Conceptualization—C,-H.T., Investigation, Data curation, Conceptualization—S.-C.L. All authors have read and agreed to the published version of the manuscript.

**Funding:** The research described in this paper was supported by grants from the National Science and Technology Council (NSTC-112-2923-B-006-0016-028), Taiwan, and An Nan Hospital (ANHRF113-37, ANHRF114-43, and ANHRF114-49), Taiwan. This research also received support from the mutual funds allocated for the Taiwan-Latvia-Lithuania cooperative project. The funding bodies for this research played no part in the study's design, data acquisition, analyses, or interpretation of the findings.

**Data availability:** Data are available on request from the corresponding author.

**Conflicts of interest:** The authors declare that the research was conducted in the absence of any commercial or financial relationships that could be construed as a potential conflict of interest.:

## Abbreviations

The following abbreviations are used in this manuscript:

| | |
|---|---|
| AC | Action current |
| ACE | Angiotensin II converting enzyme |
| AP | Action potential |
| AT1 | Angiotensin II type 1 receptor |
| DRG | Dorsal root ganglion |
| $EC_{50}$ | Half-maximal stimulation |
| EUG | Eugenol |
| Iapp | Applied current |
| $I_{Na}$ | Voltage-gated $Na^+$ current |
| $I_{Na(NI)}$ | Non-inactivating (persistent) $Na^+$ current |
| $Na_V$ channel | Voltage-gated $Na^+$ channel |
| PPAR-γ | Peroxisome proliferator-activated receptor |
| PVIN | Parvalbumin-expressing interneuron |
| Ran | Ranolazine |
| SO | Subthreshold oscillation |
| SS | Somatic spiking |
| TEL | Telmisartan |
| $V$ | Membrane potential |

## References

1. Lacourcière, Y.; Tytus, R.; O'Keefe, D.; Lenis, J.; Orchard, R.; Martin, K. Efficacy and tolerability of a fixed-dose combination of telmisartan plus hydrochlorothiazide in patients uncontrolled with telmisartan monotherapy. *J. Hum. Hypertens.* **2001**, *15*, 763–770. https://doi.org/10.1038/sj.jhh.1001267.
2. Burnier, M. Telmisartan: a different angiotensin II receptor blocker protecting a different population? *J. Int. Med. Res.* **2009**, *37*, 1662-1679. doi: 10.1177/147323000903700602.
3. Williams, B.; Lacourcière, Y.; Schumacher, H.; Gosse, P.; Neutel, J.M. Antihypertensive efficacy of telmisartan vs ramipril over the 24-h dosing period, including the critical early morning hours: a pooled analysis of the PRISMA I and II randomized trials. *J. Hum. Hypertens.* **2009**, *23*, 610–619. https://doi.org/10.1038/jhh.2009.4.

 doi:10.20944/preprints202603.0533.v1




4. Michel, M.C.; Brunner, H.R.; Foster, C.; Huo, Y. Angiotensin II type 1 receptor antagonists in animal models of vascular, cardiac, metabolic and renal disease. *Pharmacol. Ther.* **2016**, *164*, 1-81. doi: 10.1016/j.pharmthera.2016.03.019.
5. Quan, W.; Zhang, S.X.; Zhang, X.Y.; Chen, X.; Yang, C.; Li, Z.Y.; Hu, R. The application of telmisartan in central nervous system disorders. *Pharmacol. Rep.* **2025**, *77*, 1196-1216. doi: 10.1007/s43440-025-00737-2.
6. Yamagishi, S.; Nakamura, K.; Matsui, T. Potential utility of telmisartan, an angiotensin II type 1 receptor blocker with peroxisome proliferator-activated receptor-gamma (PPAR-gamma)-modulating activity for the treatment of cardiometabolic disorders. *Curr. Mol. Med.* **2007**, *7*, 463-469. doi: 10.2174/156652407781387073.
7. Singh, B.; Sharma, B.; Jaggi, A.S.; Singh, N. Attenuating effect of lisinopril and telmisartan in intracerebroventricular streptozotocin induced experimental dementia of Alzheimer's disease type: possible involvement of PPAR-γ agonistic property. *J. Renin Angiotensin Aldosterone Syst.* **2013**, *14*, 124-136. doi: 10.1177/1470320312459977.
8. Gao, Y.; Li, W.; Liu, Y.; Wang, Y.; Zhang, J.; Li, M.; Bu, M. Effect of Telmisartan on Preventing Learning and Memory Deficits Via Peroxisome Proliferator-Activated Receptor-γ in Vascular Dementia Spontaneously Hypertensive Rats. *J. Stroke Cerebrovasc. Dis.* **2018**, *27*, 277-285. doi: 10.1016/j.jstrokecerebrovasdis.2017.01.025.
9. Abdel Rasheed, N.O.; Ibrahim, W.W. Telmisartan neuroprotective effects in 3-nitropropionic acid Huntington's disease model in rats: Cross talk between PPAR-γ and PI3K/Akt/GSK-3β pathway. *Life Sci.* **2022**, *297*, 120480. doi: 10.1016/j.lfs.2022.120480.
10. Fu, X.X.; Wei, B.; Cao, H.M.; Duan, R.; Deng, Y.; Lian, H.W.; Zhang, Y.D.; Jiang, T. Telmisartan Alleviates Alzheimer's Disease-Related Neuropathologies and Cognitive Impairments. *J. Alzheimers Dis.* **2023**, *94*, 919-933. doi: 10.3233/JAD-230133.
11. Kurinami, H.; Shimamura, M.; Sato, N.; Nakagami, H.; Morishita, R. Do angiotensin receptor blockers protect against Alzheimer's disease? *Drugs Aging* **2013**, *30*, 367-372. doi: 10.1007/s40266-013-0071-2.
12. Abdelkader, N.F.; Abd El-Latif, A.M.; Khattab, M.M. Telmisartan/17β-estradiol mitigated cognitive deficit in an ovariectomized rat model of Alzheimer's disease: Modulation of ACE1/ACE2 and AT1/AT2 ratio. *Life Sci.* **2020**, *245*, 117388. doi: 10.1016/j.lfs.2020.117388.
13. Abo-Youssef, A.M.; Khallaf, W.A.; Khattab, M.M.; Messiha, B.A.S. The anti-Alzheimer effect of telmisartan in a hyperglycemic ovariectomized rat model; role of central angiotensin and estrogen receptors. *Food Chem. Toxicol.* **2020**, *142*, 111441. doi: 10.1016/j.fct.2020.111441.
14. Hu, W.; Li, Y.; Zhao, Y.; Dong, Y.; Cui, Y.; Sun, S.; Gong, G.; Zhang, H.; Chai, Q.; Wang, J.; Liu, Z. Telmisartan and Rosuvastatin Synergistically Ameliorate Dementia and Cognitive Impairment in Older Hypertensive Patients With Apolipoprotein E Genotype. *Front. Aging Neurosci.* **2020**, *12*, 154. doi: 10.3389/fnagi.2020.00154.
15. Khalifa, M.;l Safar, M.M.; Abdelsalam, R.M.; Zaki, H.F. Telmisartan Protects Against Aluminum-Induced Alzheimer-like Pathological Changes in Rats. *Neurotox. Res.* **2020**, *37*, 275-285. doi: 10.1007/s12640-019-00085-z.
16. Kehoe, P.G.; Turner, N.; Howden, B.; Jarutyte, L.; Clegg, S.L.; Malone, I.B.; Barnes, J.; Nielsen, C.; Sudre, C.H.; Wilson, A.; Thai, N.J.; Blair, P.S.; Coulthard, E.; Lane, J.A.; Passmore, P.; Taylor, J.; Mutsaerts, H.J.; Thomas, D.L.; Fox, N.C.; Wilkinson, I.; Ben-Shlomo, Y.; RADAR investigators. Safety and efficacy of losartan for the reduction of brain atrophy in clinically diagnosed Alzheimer's disease (the RADAR trial): a double-blind, randomised, placebo-controlled, phase 2 trial. *Lancet Neurol.* **2021**, *20*, 895-906. doi: 10.1016/S1474-4422(21)00263-5.
17. Liu, C.H.; Sung, P.S.; Li, Y.R.; Huang, W.K.; Lee, T.W.; Huang, C.C.; Lee, T.H.; Chen, T.H.; Wei, Y.C. Telmisartan use and risk of dementia in type 2 diabetes patients with hypertension: A population-based cohort study. *PLoS Med.* **2021**, *18*, e1003707. doi: 10.1371/journal.pmed.1003707.
18. Said, E.S.; Elsayed, A.M.; Rashed, L.A.; Nadwa, E.H.; Alsuhaibani, N.A.; Alfuraih, B.S.; Mahmoud, R.H. Evaluation of nootropic activity of telmisartan and metformin on diazepam-induced cognitive dysfunction in mice through AMPK pathway and amelioration of hippocampal morphological alterations. *Eur. J. Pharmacol.* **2021**, *912*, 174511. doi: 10.1016/j.ejphar.2021.174511.

 doi:10.20944/preprints202603.0533.v1




19. Kuber, B.; Fadnavis, M.; Chatterjee, B. Role of angiotensin receptor blockers in the context of Alzheimer's disease. *Fundam. Clin. Pharmacol.* **2023**, *37*, 429-445. doi: 10.1111/fcp.12872.
20. Zhang, P.; Hou, Y.; Tu, W.; Campbell, N.; Pieper, A.A.; Leverenz, J.B.; Gao, S.; Cummings, J.; Cheng, F. Population-based discovery and Mendelian randomization analysis identify telmisartan as a candidate medicine for Alzheimer's disease in African Americans. *Alzheimers Dement.* **2023**, *19*, 1876-1887. doi: 10.1002/alz.12819.
21. Madani, A.F.; Syauqi, M.A.; Permatasari, J.A.; Putri, A.A.; M, F.; Permana A.D. Development of Telmisartan Nanocrystal-Based Dissolving Microneedle for Brain Targeting via Trigeminal Pathway: A Potentially Promising Treatment for Alzheimer's with an Improved Pharmacokinetic Profile. *ACS Appl. Bio. Mater.* **2024**, *7*, 2582-2593. doi: 10.1021/acsabm.4c00246.
22. Altun, S.; Özdemir, S.; Arslan, H.; Kiliçlioğlu, M.; Yaprak, E.; Bolat, İ.; Aydın, Ş. Impact of long-term deltamethrin exposure on Alzheimer's-related neurodegeneration in rats. *Exp. Neurol.* **2025**, *388*, 115223. doi: 10.1016/j.expneurol.2025.115223.
23. Noto, N.M.; Robison, L.S.; Speth, R.C. Chronic Treatment of a Mouse Model of Cerebral Amyloid Angiopathy and Brain AT1 Receptor Expression. *bioRxiv* [Preprint] **2025**, 2025.05.16.654535. doi: 10.1101/2025.05.16.654535.
24. Romanova, D.Y.; Balaban, P.M.; Nikitin, E.S. Sodium Channels Involved in the Initiation of Action Potentials in Invertebrate and Mammalian Neurons. *Biophysica* **2022**, *2*, 184-193. https://doi.org/10.3390/biophysica2030019.
25. Catterall, W.A. Voltage-gated sodium channels at 60: structure, function and pathophysiology. *J. Physiol.* **2012**, *590*, 2577-2589. doi: 10.1113/jphysiol.2011.224204.
26. de Lera Ruiz, M, Kraus, R.L. Voltage-Gated Sodium Channels: Structure, Function, Pharmacology, and Clinical Indications. *J. Med. Chem.* **2015**, *58*, 7093-7118. doi: 10.1021/jm501981g.
27. Wengert, E.R.; Patel, M.K. The Role of the Persistent Sodium Current in Epilepsy. *Epilepsy Curr.* **2021**, 21, 40-47. doi: 10.1177/1535759720973978.
28. Huang, H.Y.; Huang, Y.B.; Wu, C.L.; Wu, S.N. Modulatory impact of tefluthrin, telmisartan, and KB-R7943 on voltage-gated $Na^+$ currents. *Biophysica* **2024**, *4*, 488-506. https://doi.org/10.3390/biophysica4040032.
29. Cheng, Y.; Wang, X.; Zhang, Q.; Ge, R.; Zhou, M.; Dai, Y. Multiple patterns of persistent inward currents with multiple types of repetitive firings in medullary serotonergic neurons of mice: An experimental and modeling study. *PLoS Comput. Biol.* **2025**, *21*, e1012918. doi: 10.1371/journal.pcbi.1012918.
30. Chou, C.J.; Cheung, C.W.; Lee, C.C.; Wu, S.N, Liutkeviciene R, Rovite V, So EC. Evidence for effective suppression of INa and $I_{K(DR)}$ by AS2034178 (bis{2-[(4-{(4′-(2-hydroxyethoxy)-2′-methyl[1,1′-biphenyl]-3-yl)methoxy}phenyl]methyl]-3,5-dioxo-1,2,4-oxadiazolidin-4-ide} tetrahydrate), an agonist of free fatty acid receptor. *Neurosci. Lett.* **2025**, *855*, 138222. doi: 10.1016/j.neulet.2025.
31. Iigaya, K.; Onimaru, H.; Ikeda, K.; Iizuka, M.; Izumizaki, M. Cellular mechanisms of synchronized rhythmic burst generation in the ventromedial hypothalamus. *Pflugers Arch.* **2025**, *477*, 131-145. doi: 10.1007/s00424-024-03031-x.
32. Ascoli, A.; Demirkol, A.S.; Tetzlaff, R.; Chua, O. Edge of Chaos Theory Sheds Light Into the All-to-None Phenomenon in Neurons—Part I: On the Fundamental Role of the Sodium Ion Channel. *IEEE Trans. Circuits Syst. I Reg. Papers* **2024**, *71*, 5-19. doi: 10.1109/TCSI.2023.3339240.
33. Jia, Y.; Gu, H, Wang, X.; Li, Y. Fast excitatory modulations paradoxically reduce spiking activity in the network and single neuron with autapse: complex bifurcations and unstable limit cycle. *Chao Solitions & Fractals* **2025**, *199*, 116752.
34. Lai, M.C.; Wu, S.N.; Huang, C.W. Telmisartan, an Antagonist of Angiotensin II Receptors, Accentuates Voltage-Gated $Na^+$ Currents and Hippocampal Neuronal Excitability. *Front. Neurosci.* **2020**, *14*, 902. doi: 10.3389/fnins.2020.00902.
35. Kouri, M.; Adamo, D.; Vardas, E.; Georgaki, M.; Canfora, F.; Mignogna, M.D.; Nikitakis, N. Small Fiber Neuropathy in Burning Mouth Syndrome: A Systematic Review. *Int. J. Mol. Sci.* **2024**, *25*, 11442. doi: 10.3390/ijms252111442.
36. Kemmer, G.; Keller, S. Nonlinear least-squares data fitting in Excel spreadsheets. *Nat. Protoc.* **2010**, *5*, 267-281. doi: 10.1038/nprot.2009.182.

 doi:10.20944/preprints202603.0533.v1




37. Wu, S.N.; Chen, B.S.; Hsu, T.I.; Peng, H.; Wu, Y.H.; Lo, Y.C. Analytical studies of rapidly inactivating and noninactivating sodium currents in differentiated NG108-15 neuronal cells. *J. Theor. Biol.* **2009**, *259*, 828-836. doi: 10.1016/j.jtbi.2009.05.003.
38. Brown, A.M. Simulation of axonal excitability using a Spreadsheet template created in Microsoft Excel. *Comput. Methods Programs Biomed.* **2000**, *63*, 47-54. doi: 10.1016/s0169-2607(00)00076-6.
39. Huang, C.W.; Chow, J.C.; Tsai, J.J.; Wu, S.N. Characterizing the effects of Eugenol on neuronal ionic currents and hyperexcitability. *Psychopharmacology* (Berl) **2012**, *221*, 575-587. doi: 10.1007/s00213-011-2603-y.
40. So, E.C.; Wu, S.N.; Lo, Y.C.; Su, K. Differential regulation of tefluthrin and telmisartan on the gating charges of $I_{Na}$ activation and inactivation as well as on resurgent and persistent $I_{Na}$ in a pituitary cell line ($GH_3$). *Toxicol. Lett.* **2018**, *285*, 104-112. doi: 10.1016/j.toxlet.2018.01.002.
41. Kim, H.K.; Youm, J.B.; Lee, S.R.; Lim, S.E.; Lee, S.Y.; Ko, T.H.; Long L.T.; Nilius, B.; Won D.N.; Noh, J.H.; Ko, K.S.; Rhee, B.D.; Kim, N.; Han, J. The angiotensin receptor blocker and PPAR-γ agonist, telmisartan, delays inactivation of voltage-gated sodium channel in rat heart: novel mechanism of drug action. *Pflugers Arch.* **2012**, *464*, 631-643. doi: 10.1007/s00424-012-1170-3.
42. Wu, S.N.; Liu, S.I.; Huang, M.H. Cilostazol, an inhibitor of type 3 phosphodiesterase, stimulates large-conductance, calcium-activated potassium channels in pituitary $GH_3$ cells and pheochromocytoma PC12 cells. *Endocrinology* **2004**, *145*, 1175-1184. doi: 10.1210/en.2003-1430.
43. Chang, T.T.; Yang, C.J.; Lee, Y.C.; Wu, S.N. Stimulatory Action of Telmisartan, an Antagonist of Angiotensin II Receptor, on Voltage-Gated $Na^+$ Current: Experimental and Theoretical Studies. *Chin. J. Physiol.* **2018**, *61*, 1-13. doi: 10.4077/CJP.2018.BAG516.
44. Amran, M.S.; Homma, N.; Hashimoto, K. Pharmacology of KB-R7943: a $Na^+$-$Ca^{2+}$ exchange inhibitor. *Cardiovasc. Drug Rev.* **2003**, *21*, 255-276. doi: 10.1111/j.1527-3466.2003.tb00121.x.
45. Wu, S.N.; Yu, M.C. Inhibition of Voltage-Gated $Na^+$ Currents Exerted by KB-R7943 (2-[2-[4-(4-nitrobenzyloxy)phenyl]ethyl]isothiourea), an Inhibitor of $Na^+$-$Ca^{2+}$ Exchanging Process. *Int. J. Mol. Sci.* **2023**, *24*, 1805. doi: 10.3390/ijms24021805.
46. Ma, X.; Miraucourt, L.S.; Qiu, H.; Sharif-Naeini, R.; Khadra, A. Modulation of SK Channels via Calcium Buffering Tunes Intrinsic Excitability of Parvalbumin Interneurons in Neuropathic Pain: A Computational and Experimental Investigation. *J. Neurosci.* **2023**, *43*, 5608-5622. doi: 10.1523/JNEUROSCI.0426-23.2023.
47. Ognjanovski, N.; Schaeffer, S.; Wu, J.; Mofakham, S.; Maruyama, D.; Zochowski, M.; Aton, S.J. Parvalbumin-expressing interneurons coordinate hippocampal network dynamics required for memory consolidation. *Nat. Commun.* **2017**, *8*, 15039. doi: 10.1038/ncomms15039.
48. Moustafa, M.; Mousa, M.H.; Saad, M.S.; Basha, T.; Elbasiouny, S.M. Bifurcation analysis of motoneuronal excitability mechanisms under normal and ALS conditions. *Front. Cell. Neurosci.* **2023**, *17*, 1093199. doi: 10.3389/fncel.2023.1093199.
49. Kar, R.; Yadav, A.; Chandrasekar, V.K.; Senthilkumar, D.V. Effect of higher-order interactions on chimera states in two populations of Kuramoto oscillators. *Chaos* **2024**, *34*, 023110. doi: 10.1063/5.0181279.
50. White, J.A.; Budde, T.; Kay, A.R. A bifurcation analysis of neuronal subthreshold oscillations. *Biophys. J.* **1995**, *69*, 1203-17. doi: 10.1016/S0006-3495(95)79995-7.
51. Hung, T.Y.; Wu, S.N.; Huang, C.W. Concerted suppressive effects of carisbamate, an anti-epileptic alkyl-carbamate drug, on voltage-gated $Na^+$ and hyperpolarization-activated cation currents. *Front. Cell. Neurosci.* **2023**, *17*, 1159067. doi: 10.3389/fncel.2023.1159067.
52. Lu, T.L.; Wu, S.N. Investigating the Impact of Selective Modulators on the Renin-Angiotensin-Aldosterone System: Unraveling Their Off-Target Perturbations of Transmembrane Ionic Currents. *Int. J. Mol. Sci.* **2023**, *24*, 14007. doi: 10.3390/ijms241814007.
53. Ohno, K.; Amano, Y.; Kakuta, H.; Niimi, T.; Takakura, S.; Orita, M.; Miyata, K.; Sakashita, H.; Takeuchi, M.; Komuro, I.; Higaki, J.; Horiuchi, M.; Kim-Mitsuyama, S.; Mori, Y.; Morishita, R.; Yamagishi, S.; Unique "delta lock" structure of telmisartan is involved in its strongest binding affinity to angiotensin II type 1 receptor. *Biochem. Biophys. Res. Commun.* **2011**, *404*, 434-437. doi: 10.1016/j.bbrc.2010.11.139.

 doi:10.20944/preprints202603.0533.v1




54. Glynn, P.; Musa, H.; Wu, X.; Unudurthi, S.D.; Little, S.; Qian, L.; Wright, P.J.; Radwanski, P.B.; Gyorke, S.; Mohler, P.J.; Hund, T.J. Voltage-gated sodium channel phosphorylation at ser571 regulates late current, arrhythmia, and cardiac function in vivo. *Circulation* **2015**, *312*, 567-577.
55. Chang, W.T.; Wu, S.N. Activation of voltage-gated sodium current and inhibition of *erg*-mediated potassium current caused by telmisartan, an antagonist of angiotensin II type-1 receptor, in HL-1 atrial cardiomyocytes. *Clin. Exp. Pharmacol. Physiol.* **2018**, *45*, 797-807. doi: 10.1111/1440-1681.12943.
56. Alonso, S.; Alvarez-Lacalle, E.; Bragard, J.; Echebarria, B. Biophysical Modeling of Cardiac Cells: From Ion Channels to Tissue. *Biophysica* **2025**, *5*, 5. https://doi.org/10.3390/biophysica5010005
57. Clancy, C.E.; Rudy, Y. $Na^+$ channel mutation that causes both Brugada and long-QT syndrome phenotypes: a simulation study of mechanism. *Circulation* **2002**, **105**, 1208-13. doi: 10.1161/hc1002.105183.
58. Chang, Y.L.; Chou, C.H.; Li, Y.F, Huang LC, Kao Y, Hueng DY, Tsai CK. Antiproliferative and apoptotic effects of telmisartan in human glioma cells. *Cancer Cell Int.* **2023**, *23*, 111. doi: 10.1186/s12935-023-02963-1.
59. Quan, W.; Xu, C.S.; Ma, C.; Chen, X.; Yu, D.H.; Li, Z.Y.; Wang, D.W.; Tang, F.; Wan, G.P.; Wan, J.; Wang, Z.F.; Li, Z.Q. Anti-tumor effects of telmisartan in glioma-astrocyte non-contact co-cultures: A critical role of astrocytic IL-6-mediated paracrine growth promotion. *Int. Immunopharmacol.* **2024**, *139*, 112707. doi: 10.1016/j.intimp.2024.112707.
60. Giammello, F.; Biella, C.; Priori, E.C.; Filippo, M.A.D.S.; Leone, R.; D'Ambrosio, F.; Paterno,' M.; Cassioli, G.; Minetti, A.; Macchi, F.; Spalletti, C.; Morella, I.; Ruberti, C.; Tremonti, B.; Barbieri, F.; Lombardi, G.; Brambilla, R.; Florio, T.; Galli, R.; Rossi, P.; Brandalise, F. Modulating voltage-gated sodium channels to enhance differentiation and sensitize glioblastoma cells to chemotherapy. *Cell Commun. Signal.* **2024**, *22*, 434. doi: 10.1186/s12964-024-01819-z.
61. Wang, J.G.; Palmer, B.F.; Vogel Anderson, K.; Sever, P. Amlodipine in the current management of hypertension. *J. Clin. Hypertens* (Greenwich) **2023**, *25*, 801-807. doi: 10.1111/jch.14709.
62. Desai, P.B.; Patel, K.; Patel, C.N.; Chaudhary, P.K. The Role of Azelnidipine and Telmisartan in Managing Stage-II Hypertension: A Comprehensive Review. *Int. J. Innov. Sci. Res. Technol.* (IJISRT) **2025**, *10*, 1394-1396, https://doi.org/10.38124/ijisrt/25apr189.
63. Chauhan, S.; Bhandari, U.; Habib, A. Efficacy of Dapagliflozin and Telmisartan Combination Therapy in Reducing Albuminuria and Inflammatory Markers in Diabetic Nephropathy: A Prospective Observational Study. *Curr. Vasc. Pharmacol.* **2025**, *23*, 441-450. doi: 10.2174/0115701611361265250211062540.
64. Philippaert, K.; Kalyaanamoorthy, S.; Fatehi, M.; Long, W.; Soni, S.; Byrne, N.J.; Barr, A.; Singh, J.; Wong, J.; Palechuk, T.; Schneider, C.; Darwesh, A.M.; Maayah, Z.H.; Seubert, J.M.; Barakat, K.; Dyck, J.R.B.; Light, P.E. Cardiac Late Sodium Channel Current Is a Molecular Target for the Sodium/Glucose Cotransporter 2 Inhibitor Empagliflozin. *Circulation* **2021**, *143*, 2188-2204. doi: 10.1161/CIRCULATIONAHA.121.053350.
65. Hao, K.; Chen, Y.; Cao, Y.; Yu, D.; Liu, X.; Wang, G. Pharmacokinetic-pharmocodynamic modeling of telmisartan using an indirect response model in spontaneously hypertensive rats. *Acta Pharmacol. Sin.* **2007**, 28, 738-743.
66. Stangier, J.; Schmid, J.; Türck, D.; Switek, H.; Verhagen, A.; Peeters, P.A.; van Marle, S.P.; Tamminga, W.J.; Sollie, F.A.; Jonkman, J.H. Absorption, metabolism, and excretion of intravenously and orally administered [$^{14}$C]telmisartan in healthy volunteers. *J. Clin. Pharmacol.* **2000**, *40*(12 Pt 1), 1312-22.
67. Wang, B.; Sheng, L.; Li, Y. Simultaneous determination of telmisartan and amlodipine in dog plasma by LC-MS-MS. J. Chromatogr. Sci. **2015**, *53*, 1708-1713. doi: 10.1093/chromsci/bmv078.
68. Lin, M.H.; Lin, J.F.; Yu, M.C.; Wu, S.N.; Wu, C.L.; Cho, H.Y. Characterization in Potent Modulation on Voltage-Gated $Na^+$ Current Exerted by Deltamethrin, a Pyrethroid Insecticide. *Int. J. Mol. Sci.* **2022**, *23*, 14733. doi: 10.3390/ijms232314733.
69. Wu, S.N. Ion Channels as a Potential Target in Pharmaceutical Designs. *Int. J. Mol. Sci.* **2023**, *24*, 6484. doi: 10.3390/ijms24076484.
70. Diez-Sepulveda, J.C.; Uribe-Buritica, F.L.; Angel-Isaza, A.M.; Bustamante-Cristancho, L.A.; Mejia-Herrera, F.; Watts-Pajaro, F.A.; Rojas-Martinez, M.F. An 80-Year-Old Woman with Alzheimer Disease and Accidental Poisoning with Pyrethroid Pesticide Successfully Treated with Intravenous Lipid Emulsion. *Am. J. Case Rep.* **2021**, *22*. e928420. doi: 10.12659/AJCR.928420.

 doi:10.20944/preprints202603.0533.v1



71. Iteire, K.A.; Sowole, A.T.; Ogunlade, B. Exposure to pyrethroids induces behavioral impairments, neurofibrillary tangles and tau pathology in Alzheimer's type neurodegeneration in adult Wistar rats. *Drug Chem. Toxicol.* **2022**, *45*, 839-849. doi: 10.1080/01480545.2020.1778020.
72. Guan, T.; Li, N.; Gao, Y.; Gao, M.; Hu, Q.; Gao, Y.; Xiao, L.; Yang, Z.; Liu, Q. Probing the potential mechanism of permethrin exposure on Alzheimer's disease through enantiomer-specific network toxicology, multi-spectroscopic, and docking approaches. *Chemosphere* **2024**, *369*, 143786. doi: 10.1016/j.chemosphere.2024.143786.
73. Dutra-Tavares, A.C.; Maia, J.G.; de Souza, T.P.; Filgueiras, C.C.; Ribeiro-Carvalho, A.; Manhães, A.C.; Abreu-Villaça, Y. Telmisartan mitigates behavioral and cytokine level alterations but impairs spatial working memory in a phencyclidine-induced mouse model of schizophrenia. *Psychopharmacology* (Berl) **2025**, *242*, 2417-2434. doi: 10.1007/s00213-025-06805-y.
74. Liu, C.H.; Tsai, M.L.; Yang, N.I.; Chang, T.Y.; Chen, T.H.; Wei, Y.C. Risks of dementia and stroke in patients with hypertension using telmisartan or other renin-angiotensin system inhibitors. *Alzheimers Dement.* **2026**, *22*, e71153. doi: 10.1002/alz.71153.